



Research article

Analysis of ball milling time to produce self-lubricating copper-tungsten disulfide composite: best trade-off between tribological performance and electrical properties

Marco Freschi^a, Matteo Di Virgilio^{a,*}, Luca Andena^a, Marco Mariani^b, Oskari Haiko^c, Jukka Kömi^c, Nora Lecis^b, Giovanni Dotelli^a

^a Department of Chemistry, Materials and Chemical Engineering "Giulio Natta", Politecnico di Milano, Piazza Leonardo Da Vinci 32, 20133 Milan, Italy

^b Department of Mechanical Engineering, Politecnico di Milano, Via La Masa 1, 20156 Milan, Italy

^c Materials and Mechanical Engineering, Centre for Advanced Steels Research, University of Oulu, Pentti Kaiteran katu 1, 90570 Oulu, Finland

ARTICLE INFO

Keywords:

Ball milling
Powder metallurgy
Sintering
Metal matrix composites
Friction
Wear resistance
Electrical conductivity

ABSTRACT

Ball milling is a fundamental step of powder metallurgy widely employed for composite manufacturing. This work focuses on the influence of ball milling time on the morphological, electrical, and tribological properties of self-lubricating copper-tungsten disulfide (Cu-WS₂) composites. The study investigates ball milling times between 1 and 24 h to guarantee different degrees of incorporation of WS₂ in the copper matrix. Micro-scratch and wear tests are performed to evaluate the tribological behavior. Optical, scanning electron, and confocal laser scanning microscopy analyze the scratch and wear tracks. The results show the reliability of the production process and a general improvement of the composites' mechanical properties compared to pure copper. The addition of WS₂ enhances the tribo-mechanical properties, increasing hardness and wear resistance and decreasing the friction coefficient. Shorter ball milling times result in larger WS₂ flakes distributed in the copper matrix, while longer ball milling times result in smaller and more dispersed particles. This homogeneous fine dispersion determines a difference in the composites' electrical conductivity and tribological performance, with shorter ball milling times (i.e., between 2 and 4 h) offering the best trade-off between wear behavior and electrical properties.

1. Introduction

Metal matrix composites (MMCs) are highly appealing due to their widely demonstrated suitability for various applications, such as automotive, electronics, and aerospace [1,2]. Among the most studied metal matrices, copper (Cu) is of prime importance thanks to outstanding electrical and thermal conductivity. Its combination with particles of different natures allows obtaining composites with significant improvements in tribo-mechanical properties. Several species have been investigated as fillers in copper matrix composites (CuMCs): ceramics [2–9], carbides [10–12], carbon-related materials [13–19], and sulfides [20–26]. Species belonging to the transition metal dichalcogenides (TMDs), such as molybdenum disulfide (MoS₂) and tungsten disulfide (WS₂), have proven their ability to enhance tribological behavior thanks to their quasi-2D hexagonal crystal configuration. These materials' intrinsic low shear strength helps the formation of transfer films on a

mated surface [27–31]. This specific feature categorizes them as solid lubricants, which differ from liquid ones because of their compatibility with more extreme operating conditions, e.g., vacuum, rotating systems, and high temperatures. In the latter case, WS₂ is often preferred to MoS₂ since its decomposition occurs at a temperature higher than 400 °C, guaranteeing better thermal stability [28].

Powder metallurgy is the primary production route for these advanced materials. The method generally consists of three well-established steps: an initial milling phase, aimed at blending the constituent powders in a homogenous fashion; a compaction phase, to mold the mixed solids in the desired shape (sheets, pellets, or tablets); the sintering of the compacted powders, to densify and strengthen the composite. Ball milling is a widely exploited technique for the treatment of powders [32–38], thanks to its applicability to a wide range of materials, cheapness, simplicity of control, and eco-friendliness [24, 39–42]. It can be deemed essential for composite manufacturing since it

* Corresponding author.

E-mail address: matteo.divirgilio@polimi.it (M. Di Virgilio).

favors an optimal dispersion of the involved solid phases up to the desired degree of homogenization [1,43–45]. Furthermore, it may also significantly influence the final morphology and properties of the product due to repeated plastic deformation, welding, and fracturing occurring during the process [3,46–51].

Several authors have focused on ball milling parameters (e.g., extent, rotation speed, milling media to powder ratio) and their effect on the final properties of the prepared composites. Nevertheless, the results of such analyses are material and process specific, and a generalization considering different combinations of matrix and phases, or different operating variables, is not possible [48,52–58], even though recent development in the prediction of tribological performance was enhanced by the use of machine learning [59–63].

This work aims to fill the data gap on copper-tungsten disulfide composites' wear behavior considering ball milling time and its impact on second-phase dispersion, hardness, and electrical and tribological properties. Previously, the effects of ball milling time on CuMCs mixed with various carbon-based second-phases were extensively investigated. The findings revealed a discernible threshold value for mixing time, as demonstrated in the studies below.

Afkham et al. [3] found that incorporating alumina (Al_2O_3) and silicon carbide (SiC) nanoparticles in a copper matrix through ball milling for 2 h was successful, while longer durations (6–24 h) caused fragmentation and work-hardening without improving the distribution of the second-phase. They also recognized the potential thermodynamic instability of Al_2O_3 and Cu when processed simultaneously due to the presence of copper oxide (Cu_2O) traces as a possible reaction by-product.

Jin et al. [64] observed that ball milling times of Cu-3 wt% graphite composites positively affect homogenization, cohesion, tensile strength, and micro-hardness while increasing brittleness. These observations demonstrated the need to tune the ball milling duration to produce composites with optimal features. Yue et al. [40] investigated ball milling times (1–7 h) to produce Cu-graphene nanosheets (GNSs) composites and found that five hours was the optimal duration to reach maximum uniformity, while longer times could damage the carbonaceous phase. Yoo et al. [13] prepared Cu-carbon nanotubes (CNTs) composites through ball milling and high-ratio differential speed rolling, resulting in a more uniform distribution of the CNTs, smaller grain size, and increased tensile strength and micro-hardness. Grzegorek et al. [65] determined that 8 h of ball milling was optimal for fabricating Cu-CNTs composites with improved mechanical properties and without excessively oxidizing the conductive metal particles.

In the field of copper matrix composites, there is a lack of research on the effects of ball milling on composites containing TMDs. Previous studies have focused mainly on powder analysis and have not evaluated the tribological properties of the composite materials. This study aims to address this gap by investigating the impact of ball milling time on the properties of self-lubricating copper-tungsten disulfide (Cu-WS₂) composites. Cu-WS₂ is a promising material for reducing friction and wear in energy consumption, which was estimated as 20% (approximately 10³ EJ) and 3% (around 16 EJ), respectively, by Holmberg et al. [66]. Nonetheless, one may notice the scarcity of information related to these materials in the discussed literature excursus about the study of milling time effects on the production and final characteristics of CuMCs mixed with TMDs.

This work employed a powder metallurgy approach, including mixing, cold-pressing, and solid-state pressureless sintering in an inert atmosphere. A set of Cu-WS₂ tablets with a constant 10 wt%-solid lubricant concentration was produced, varying the milling times from 1 to 24 h to achieve different degrees of homogenization between the Cu and embedded WS₂ particles. The several tests carried out, including granulometry tests, X-ray diffraction (XRD), static optical contact angle evaluation, density and electrical properties measurement, micro-scratch tests, micro-indentation hardness tests, wear tests, and optical, scanning electron, and confocal laser scanning microscopy, determined

the properties sensitivity to varying the ball milling duration. The main results are reported here, while additional characterizations and results are included in the [Supplementary Information](#). The research aims to expand the available knowledge on ball milling effects in Cu-WS₂ composites and provide insights into the optimal duration for the production and the final characteristics of the material.

2. Materials and methods

The current section outlines the materials, the sample production method, and the analysis parameters. Further investigations were conducted and reported in the [Supporting Information](#) to characterize the composite material comprehensively.

2.1. Materials

The following raw materials were employed to fabricate the Cu-WS₂ composites:

- electrolytic copper (Cu) powders characterized by a nominal particle size of 45 μm and a purity level > 99.5%, supplied by Makin Metal Powders, Rochdale, UK;
- tungsten disulfide (WS₂) micro-powders with a mean particle size of 2 μm and a 99% purity level, provided by Sigma-Aldrich Corporation, St. Louis, MO, USA

2.2. Composites production procedure

The oven G-2100 by F.LLI GALLI G. & P. snc, Milano, Italy, was used to preliminarily dry copper powders at 120 °C for 6 h to eliminate moisture traces. Then, Cu was combined with 10 wt% of WS₂ powders, and the rough mix was inserted in a polyethylene (PE) container along with zirconia spheres (diameter of 15 mm). Ball-to-powder weight ratio (BPR) was fixed at 10-to-1. Mixing and homogenization were performed via the 1-level roller ball milling system acquired from MGS S.r.l., Olginate, Italy, onto which a cylindrical porcelain alumina jar hosting the PE container was rolled at 60 rpm. Timespans of 1, 2, 4, 8, 12, and 24 h were applied to produce a set of six different composites to study the effects of this parameter on their properties. Cold-pressing was executed to compact powders in the form of tablets by filling a steel tablet-making device with 1.5 g of milled powders and subjecting it to a pressure of 6 tons for five minutes, applied through a Specac Ltd., Orpington, UK, hydraulic press. The so-obtained samples, whose diameter and thickness were 13 mm and 2 mm, respectively, were hot-sintered in an EHA Model 1200 °C E-Range Tube Furnace (Carbolite Gero Ltd., Hope, UK). A heating ramp of 8 °C min⁻¹ was used up to a temperature of 550 °C, controlled by a thermocouple to prevent unwanted WS₂ thermal decomposition (previously observed in thermogravimetric analyses on virgin WS₂ powders). This upper limit was maintained for one hour. The sintering process required an atmosphere of N₂/H₂ in a 95/5% ratio. A flow of 5 l h⁻¹ was guaranteed by two Brooks® Instrument, Hatfield, PA, USA, Smart Mass Flow Controller 5850. As the last manufacturing step, the composites were let to cool down in the switched-off furnace to room temperature. The samples were labeled as CW-X, in which X identifies the specific duration of the mixing step.

2.3. Cross-sectional analysis

The cross-sections of the composites were analyzed with the Nikon, Tokyo, Japan, Eclipse L V150NL OM optical microscope by capturing images with a magnification of 500x both at the edge and at the bulk of the cross-section of each sample. Cross-sectional SEM images of the properly polished composites were obtained using the scanning electron microscope EVO 50 EP/LZ4 PENTAFET SEM by Carl Zeiss S.p.A., Jena, Germany, at a magnification of 2000x.

2.4. Electrical properties assessment

The DC resistance-meter model 2841 by B&K Precision Corporation, Yorba Linda, CA, USA, was used to survey the samples' electrical resistances (R , Ω). The corresponding electrical resistivities (ρ , Ω m) were calculated by Eq. (1) by way of the second Ohm's law:

$$\rho = \frac{R}{l} \frac{t}{d} \quad (1)$$

The geometrical parameters, manually measured with a Fujisan digital micrometer, are the thickness of the tablet (t , m), the distance between the test clips (d , m), and the length of the chord perpendicular to the inter-distance located at the midpoint between the two clips (l , m).

2.5. Micro-scratch tests

A Micro-Scratch Tester supplied by CSM Instruments (now Anton Paar, Graz, Austria) was employed to execute micro-scratch tests. The experiments included three stages: a pre-scan, a scratch stage, and a post-scan. In the pre-scan stage, the conical Rockwell stainless steel indenter with an apex angle of 120° and a spherical diamond tip ($R = 200 \mu\text{m}$) was slid at the lowest normal load (0.03 N) to determine the surface profile of the samples. During the scratch stage, the penetration depth (P_d , mm) and tangential force (F_t , N) were measured by imposing a normal load of 15 N and by moving the indenter up to a length (l_s) of 3 mm at a fixed speed of 20 mm min^{-1} . In the end, the topography of the damaged area was studied in the post-scan stage to quantify the residual depth (R_d , mm). The outcomes of the apparent friction coefficient (FC), scratch hardness (H_s , MPa), and degree of penetration (DoP) were derived from the experimental results via Eqs. (2), (4), and (5), respectively. In detail, FC is the ratio between the tangential force and the imposed normal force:

$$FC = \frac{F_t}{F_n} \quad (2)$$

In addition to adhesion, values derived in such a way typically consider a significant contribution of deformation [67]; hence, a direct comparison with friction coefficients obtained from the wear tests cannot be made. Scratch hardness is the ratio between the normal force and the effective projected contact area (A_c , mm^2), calculated by Eq. (3) according to the geometrical sketch in Fig. S6 (Supplementary Information) [68,69]:

$$A_c = 2\pi r \sin\alpha + (P_d - R(1 - \cos\alpha)) \frac{\sin\beta}{\sin\gamma} \quad (3)$$

$$H_s = \frac{F_n}{A_c} \quad (4)$$

The degree of penetration is computed as the ratio between penetration depth (P_d , mm) and the radius (r , mm) of the contact area:

$$DoP = \frac{P_d}{r} \quad (5)$$

Post-scratch test samples were cleared from residual debris by blowing compressed air and then analyzed via the Keyence Corporation, Osaka, Japan, confocal laser scanning microscope model VK-X200 to evaluate the effects on their morphology. Optical and laser images of the scratches of each composite were acquired at 20x magnification. The geometrical investigation of the grooves' cross-sectional area (A_g , mm^2) and the corresponding ridges' cross-sectional area (A_r , mm^2) was performed through the software VK Analyzer Plus by selecting ten scanning points on the produced scratches. Eq. (6) calculates the specific wear rate (W , $\text{mm}^3 \text{ N}^{-1} \text{ m}^{-1}$) values for each composite:

$$W = \frac{(A_g - A_r)}{s_d} \frac{l_s}{F_n} \quad (6)$$

In Equation 6, l_s is the scratch length, s_d (m) is the sliding distance of 0.003 m, and F_n is the applied normal load of 15 N. Wear coefficients of each sample were estimated using Eq. (7) as the product between their corresponding specific wear rate and scratch hardness:

$$k = WH_s = \frac{(A_g - A_r)}{s_d} \frac{l_s}{F_n} H_s \quad (7)$$

2.6. Wear tests

The CSM Instruments (now Anton Paar, Graz, Austria) tribometer has enabled the execution of wear tests based on a ball-on-disk configuration. A 100Cr6 steel counter ball with a 6 mm diameter and a hardness of $831 \pm 21 \text{ HV}$ was chosen to minimize the risk of undesired deformation or destruction of the samples while producing a circular trace of radius 4.5 mm. The copper matrix composites were blown using compressed air, secured to a mandrel, and rotated at a constant tangential speed of 0.18 m s^{-1} while exerting a nominal normal load of 5 N to reproduce an overall distance of 500 m. The friction coefficient trend as a function of the covered distance was coupled with the SEM (magnifications of 150x, 1500x, and 3000x) and CLSM (magnification of 20x) inspection of the wear tracks to deduce information about the wear behavior of the manufactured composites. Following a procedure analogous to the one described in Section 2.5, the specific wear rate (W , $\text{mm}^3 \text{ N}^{-1} \text{ m}^{-1}$) of each sample was inferred via Eq. (8), where A_g (mm^2) is the wear groove cross-sectional area, A_r (mm^2) is the cross-sectional area of the corresponding ridges (both evaluated employing VK Analyzer Plus at ten different scanning points of the track), C (mm) is the track circumference, s_d (m) is the sliding distance and F_n (N) is the applied normal load:

$$W = \frac{(A_g - A_r)}{s_d} \frac{C}{F_n} \quad (8)$$

The corresponding wear coefficients were calculated via Eq. (9), in which HV (MPa) is the Vickers hardness value obtained from micro-indentation hardness tests:

$$k = WH_s = \frac{(A_g - A_r)}{s_d} \frac{C}{F_n} HV \quad (9)$$

3. Results

3.1. Cross-section analysis

Fig. 1 reports the optical microscopy (OM) images of the cross-sections of the ball-milled samples at a 500x-magnification at both the upper external surface (Fig. 1, left column) and the bulk (Fig. 1, right column). Overall, dark and bright areas emerge as well dispersed, forming elongated dark spots within the matrix. In particular, the mutual dispersion improves at longer ball milling durations, with a decrease in the agglomerates' dimensions and a more efficient distribution of the second phase around copper clusters [40,62,70]. The agglomerates are oriented perpendicularly to the press direction in the 1-hour milled sample (CW-1, Fig. 1-a). Despite their considerable dimension (up to $15 \mu\text{m}$), they do not interrupt the compact and continuous network of the copper matrix. The black areas are better and better dispersed and lowered in dimension, increasing the ball milling time up to 24 h (CW-24, Fig. 1-f). In this last case, no relevant agglomeration is detected, and the dark areas surround the copper crystals, highlighting the elongated structure of the metallic matrix.

As reported in Section S2 (Supplementary Information) about density measurements, a fraction of porosity is present in the fabricated composites. Considering that OM does not allow to distinguish if the dark areas represent the second phase or the porosity and that micro-porosity is not detectable with such a technique, a deeper analysis was carried out by means of scanning electron microscopy (SEM). Fig. 2

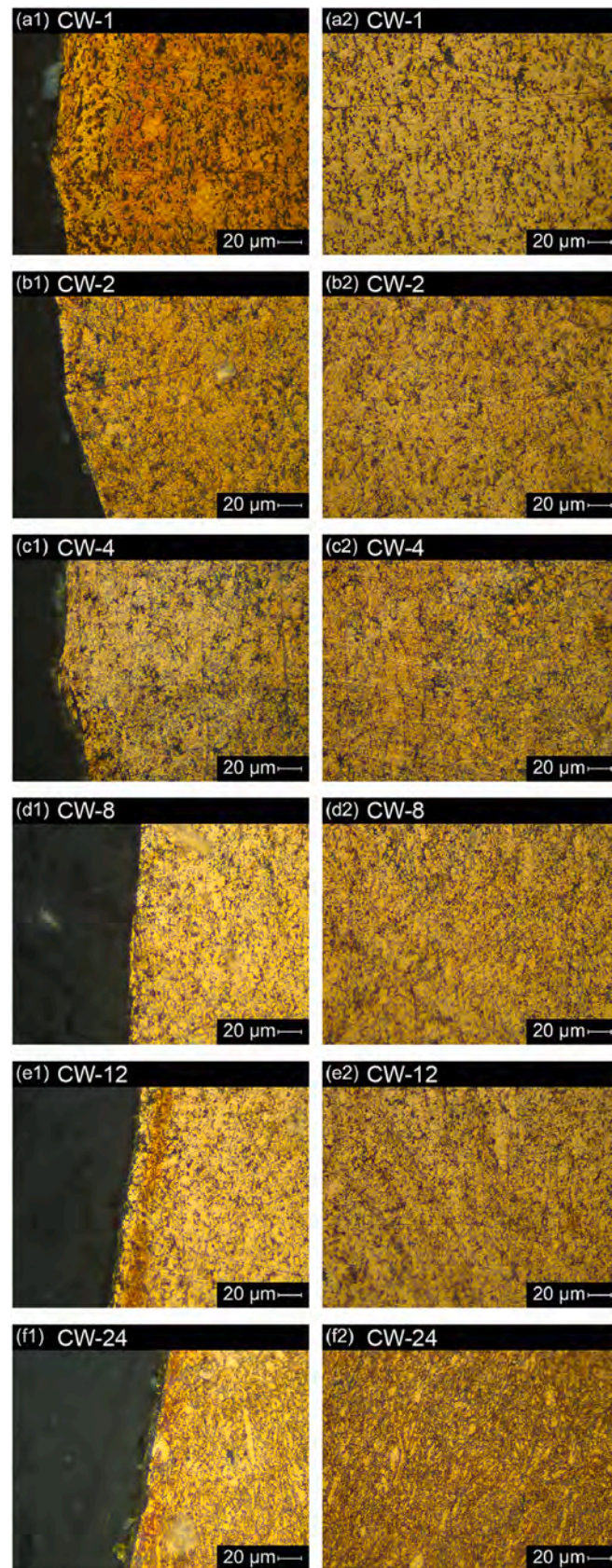


Fig. 1. OM images of the cross-section of the CW-X composites at 500x magnification: (a1) CW-1 upper edge; (a2) CW-1 bulk; (b1) CW-2 upper edge; (b2) CW-2 bulk; (c1) CW-4 upper edge; (c2) CW-4 bulk; (d1) CW-8 upper edge; (d2) CW-8 bulk; (e1) CW-12 upper edge; (e2) CW-12 bulk; (f1) CW-24 upper edge; (f2) CW-24 bulk.

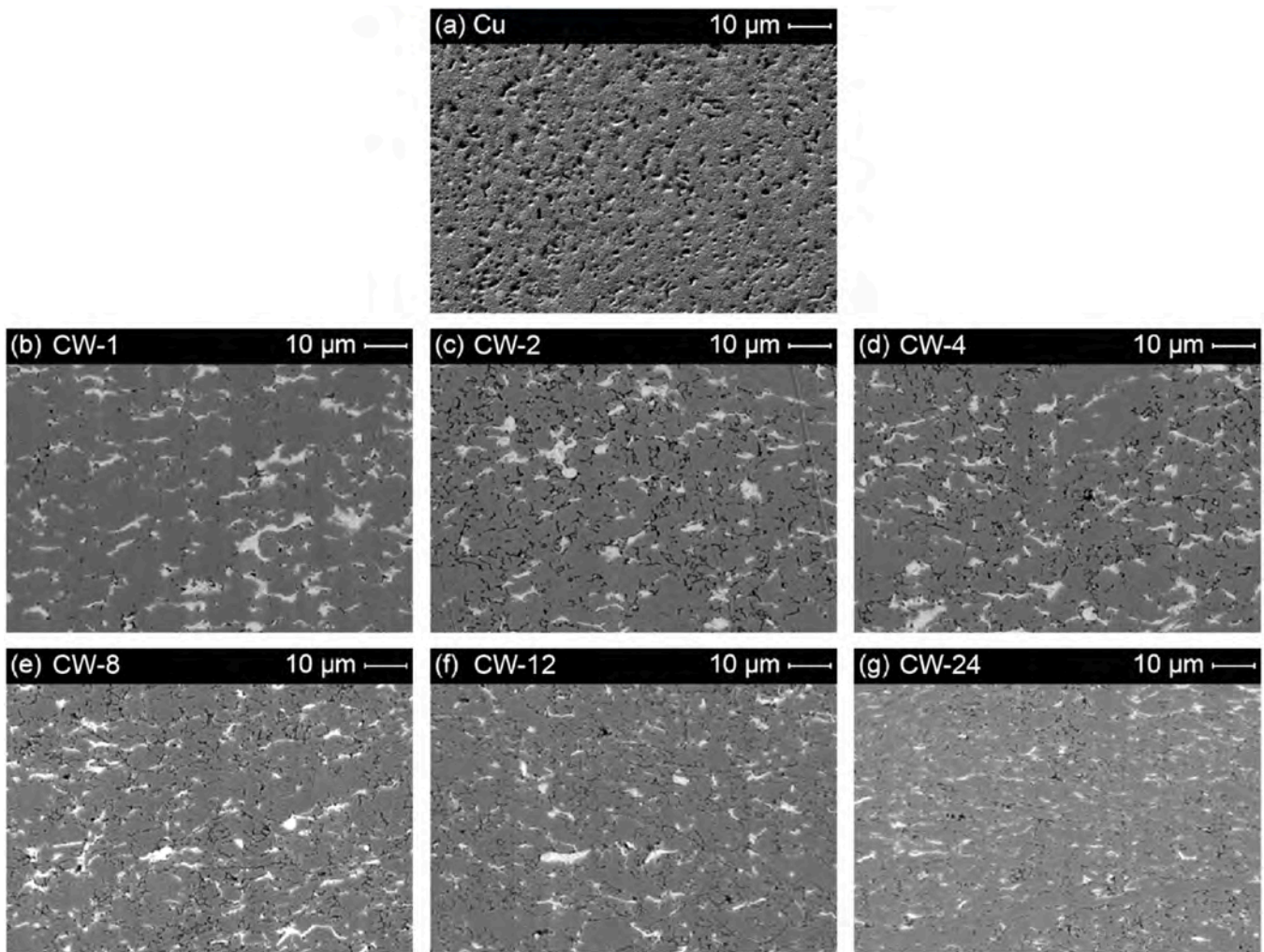


Fig. 2. SEM images of the cross-section of pristine Cu and of the CW-X composites at 2000x magnification: (a) Cu; (b) CW-1; (c) CW-2; (d) CW-4; (e) CW-8; (f) CW-12; (g) CW-24.

gathers cross-sectional SEM images of immaculate Cu and the CW-X composites at a magnification of 2000x. The reference material was compared with the as-prepared samples to highlight the milling

process's effects on the final products' microstructure. The grey phase can be identified as the copper matrix, whereas the brighter one can be recognized as the solid lubricant [71]. The homogeneous distribution of

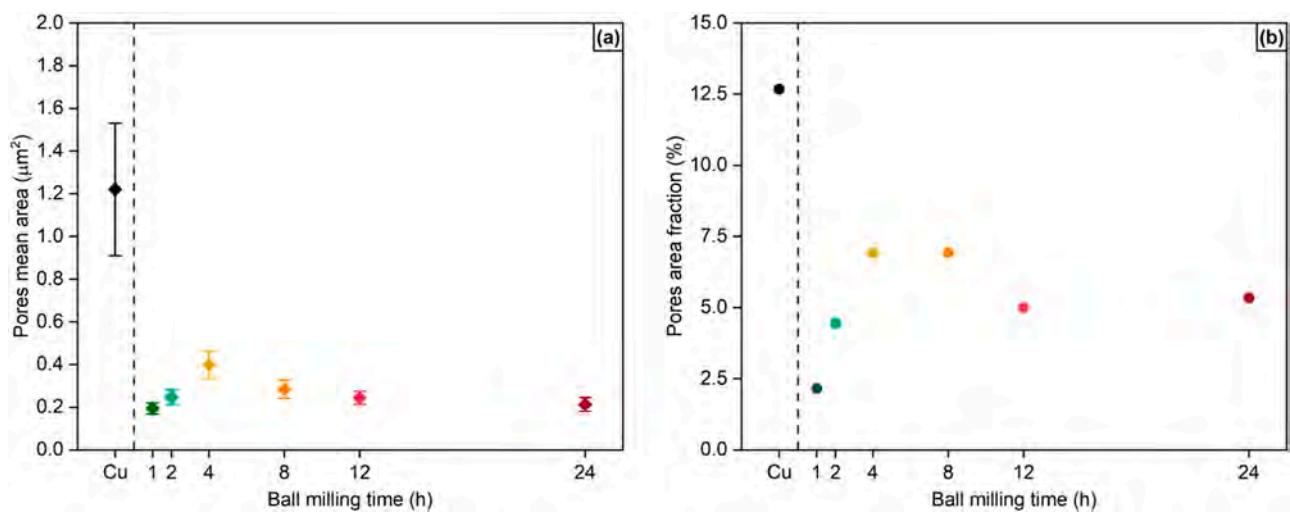


Fig. 3. (a) Evaluated mean area of the pores as a function of ball milling time; (b) Evaluated fraction of pores area with respect to cross-section area as a function of ball milling time.

the reinforcement hinders the development of undesired phases throughout the preparation and production process [72], and it guarantees the predictability and consistency of the properties of the composite material [73,74]. The better homogeneity and fine dispersion of WS₂ at longer ball milling times, supposed from OM, is confirmed by the gradual reduction of bright spots' dimensions in the SEM images of the composites [13]. The dark spots, which can be attributed to micro-porosity, seem to get smaller and smaller in the samples prepared with a longer milling process, except for CW-24. This observation is strengthened by the investigation of the pores mean area and the pores area percentage with respect to the total area of the cross-section, both qualitatively evaluated by image processing (Fig. 3). In particular, the pores mean area (Fig. 3-a) substantially decreases from pure copper to the self-lubricating composites, for which it ranges from 0.2 to 0.4 μm^2 . The pore area percentage (Fig. 3-b) increases while extending the milling duration to 8 h; however, the samples CW-12 and CW-24 exhibit intermediate values between CW-2 and CW-8. This trend can be given by an initial agglomeration of the copper powder while extending the milling time to a duration between 4 and 8 h, determining an increase in pores dimension and pores area fraction, as assessed by Fig. 3. Beyond this ball milling time, the copper clusters are fragmented, and the smaller particles better stack and fill the empty spaces during compression and sintering. The finer dimension of the copper grains as the milling time increases is qualitatively observable in Fig. 1. The restrained variability of pores mean area values are consistent with density measurements, again supporting the reproducibility of the proposed fabrication process.

3.2. Electrical resistivity

The electrical resistivity results of the CW-X composites are summarized in Fig. 4. Ball milling times longer than 4 h entail an undesired increase of resistivity up to values above $10^{-7} \Omega \text{ m}$. On the contrary, CW-1 ($5.84 \pm 1.40 \times 10^{-8} \Omega \text{ m}$) and CW-2 ($7.08 \pm 0.09 \times 10^{-8} \Omega \text{ m}$) exhibit resistivity values in the same order of magnitude as the dendritic copper powder ($2.96 \pm 0.15 \times 10^{-8} \Omega \text{ m}$) and pure copper from literature ($1.68 \times 10^{-8} \Omega \text{ m}$ [75]). Therefore, the influence of the 10 wt% of semiconducting lubricant on the electrical properties of the final composites appears to be not substantial, especially at short ball milling times, guaranteeing performance that can be deemed suitable for applications in which good electrical conduction is required.

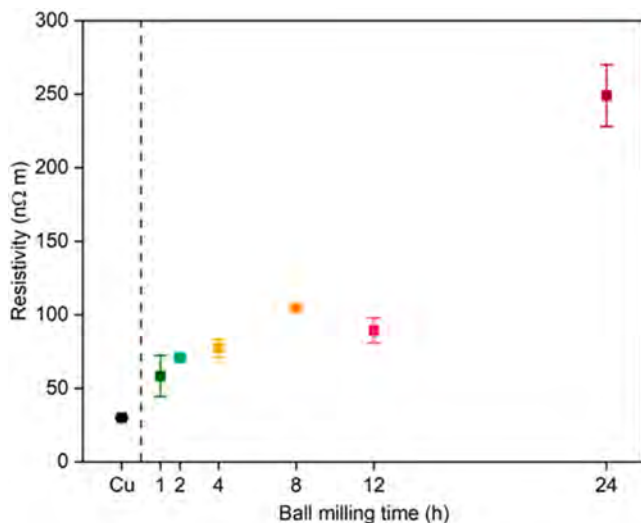


Fig. 4. Electrical resistivity values of the CW-X composites compared with pristine Cu.

3.3. Micro-scratch test results

Fig. 5 illustrates the apparent friction coefficient and scratch hardness of the CW-X samples. All composites reveal an improved friction behavior with respect to pure copper (0.604 ± 0.023), confirming a self-lubricating ability fostered by WS₂. CW-2 exhibits the lowest friction coefficient of 0.343 ± 0.019 (Fig. 5-a), closely followed by CW-24 (0.350 ± 0.020). Nevertheless, the longer ball milling time required to prepare this last sample makes it less attractive than CW-2, whose friction performance is slightly better despite having undergone a much shorter mixing step (2 h). The scratch hardness of the analyzed materials is higher than that of pristine copper ($654.8 \pm 44.8 \text{ MPa}$) up to 4 h of ball milling. CW-4 and CW-2 are the composites that guarantee the best scratch hardness performance ($758.8 \pm 23.7 \text{ MPa}$ and $758.2 \pm 17.7 \text{ MPa}$, respectively). Longer milling times induce a softening of the produced composites (Fig. 5-b), probably due to the higher dispersion of the solid lubricant and to metal particles clustering [47], again indicating that an unwanted worsening of the properties is caused at such preparation conditions as already inferred from electrical resistivity measurements (Section 3.2). The refinement of the copper grains and the interaction with WS₂ led, at first, to an increase in the strength of the material [76]. Extending the milling time, the softening of the composites was the result of the combination of a higher dispersion of WS₂, which partially hindered the coarsening of the copper powder, compromising its integrity and the inverse Hall-Petch effect. According to this effect, decreasing the grain dimension determines an increase in strength up to a certain limit, typically around 20 nm [77], after which an inversion is observed, and the strength decreases due to the shifting from dislocation slip to grain boundary sliding [78–80].

No significant flake-like debris formation close to the scratch groove borders can be appreciated from OM and confocal laser scanning microscopy (CLSM) images, illustrated in Fig. 6. Such an outcome indicates a plastic deformation capability of the composites with no chipping, which can be deemed a beneficial feature offered by the CW-X composites. This characteristic can be crucial in those applications where a rotating system is employed since debris could damage the components or, in the case of a specific component whose maintenance would be complex due to its location. The CLSM images confirm that a lower penetration is reached in the composites with respect to pristine Cu (dark blue areas). The best performance is exhibited by the CW-2 sample, whose track is uniform, shallow, and with practically negligible debris formation. Conversely, CW-24 displays the deepest groove and the thickest ridges among the composites, consistently with its lower scratch hardness ($614.3 \pm 37.3 \text{ MPa}$).

In association with the OM and CLSM, the analysis of friction coefficient and degree of penetration trends (Fig. S7, Supplementary Information) as a function of scratch length could help evaluate possible wear mechanisms. The abrasive mechanism can be classified into different categories, as indicated by Hokkirigawa and Kato [81]. Specifically, a wedge wear mechanism can be associated with unlubricated copper, confirmed by the marked wedge at the end of the scratch in Figs. 6-a2. The almost constant value of the friction coefficient (FC) in Cu, CW-1, and CW-2 is associated with a ploughing-type (or negligible) wear, while the discontinuous trends of CW-4, CW-8, CW-12, and CW-24 point to a flaking-like abrasive mechanism. Although no considerable flake debris was detected on the scratched surfaces, the irregularity of the scratch surface of these composites and the more pronounced ridges with respect to the samples characterized by a milling time of 1 or 2 h might suggest a transition toward a flaking-like abrasive mechanism. The degree of penetration (DoP) trends confirm these hypotheses since the composites prepared with longer mixing steps disclose a higher variability of the DoP during the tests. CW-1 exhibits a DoP peak at around 1 mm, probably due to the exposition to the surface of some WS₂-rich agglomerates highlighted by the cross-sectional optical microscopy. As a consequence, the indenter could have more easily penetrated the composites, contextually activating the lubricating

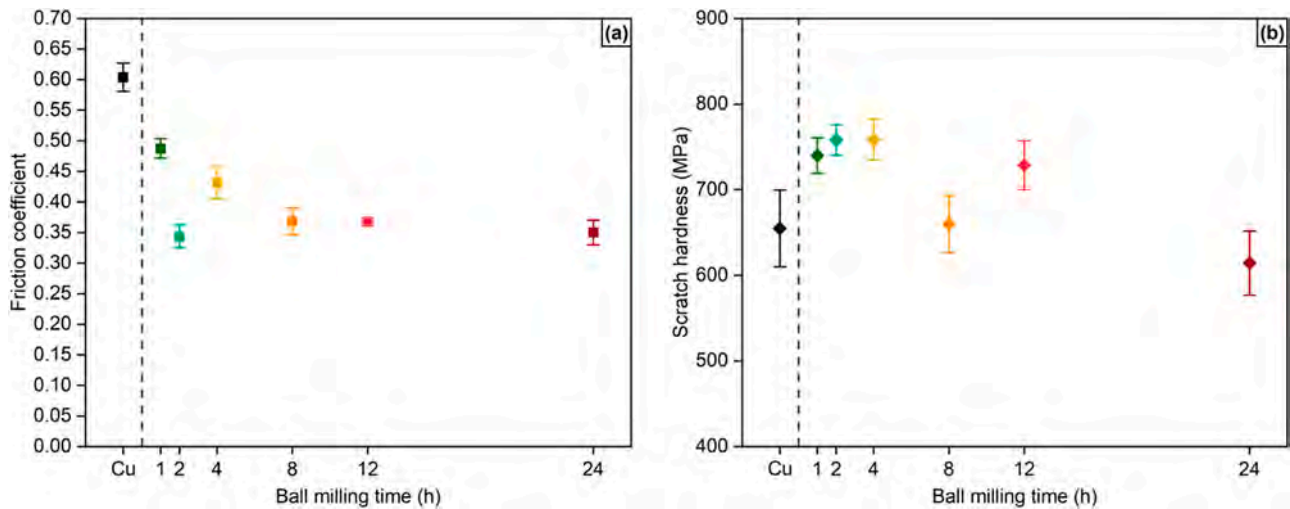


Fig. 5. (a) Friction coefficients of the CW-X composites compared with pristine Cu; (b) Scratch hardness of the CW-X composites compared with pristine Cu.

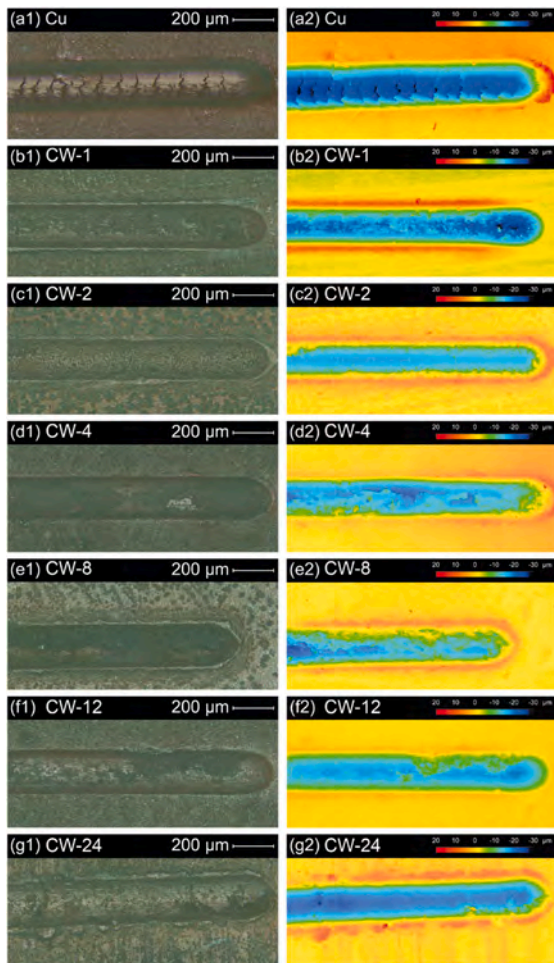


Fig. 6. Images at 20x magnification of the scratches: pristine Cu (a1) optical and (a2) laser; CW-1 (b1) optical and (b2) laser; CW-2 (c1) optical and (c2) laser; CW-4 (d1) optical and (d2) laser; CW-8 (e1) optical and (e2) laser; CW-12 (f1) optical and (f2) laser; CW-24 (g1) optical and (g2) laser.

ability of WS_2 , which can be considered as the cause of the subsequent decrease of FC at around 1.5 mm.

Specific wear rate and wear coefficient outcomes of scratch tests, derived from Eqs. (6) and (7) (Section 2.5), are reported in Fig. 7. The

enhancement promoted by WS_2 on the wear behavior of the studied composites with respect to pure copper appears evident by the strong decrease of both parameters. Concerning the specific wear rate (Fig. 7-a), the addition of WS_2 brings a 4-to-5-fold improvement in the composites prepared with a ball milling duration of less than 12 h, with the best performance guaranteed by CW-2 ($0.077 \pm 0.031 \text{ mm}^3 \text{ N}^{-1} \text{ m}^{-1}$). The same trend is observed for the wear coefficients (Fig. 7-b), with values ranging between 0.059 ± 0.024 (CW-2) and 0.117 ± 0.019 (CW-24) that outperform bare copper by 3–5 times. In general, the results indicate that, for longer milling durations, the beneficial influence of WS_2 on the wear properties of self-lubricating Cu- WS_2 composites decreases slightly.

3.4. Wear test results

The friction coefficient evolution of CW-X samples with respect to the distance covered during the wear test is highlighted in Fig. 8. All the composites demonstrate good frictional behavior as a consequence of the lubricating effect of tungsten disulfide. Friction coefficients fluctuate between 0.095 and 0.21, performances considerably better than the one recorded for a pure copper tablet (0.75, Fig. 8-a). However, the investigated composites display some dissimilarities in the overall trends (Fig. 8-b). CW-1 (green curve) and CW-8 (orange curve) have comparable behavior, with a steep friction coefficient transition up to 0.12 at around 250 m. Despite the final plateau is similar to the one of CW-2 (turquoise curve), the drop observed for this sample occurs throughout a wider distance interval and, therefore, in a more graduate fashion. Differently, CW-12 (red curve) exhibits an immediate drop up to 0.14 and a second reduction up to 0.10 at a distance range analogous to CW-2.

Nevertheless, it undergoes a friction coefficient increase up to 0.15 after 300 m. CW-4 (yellow curve) friction coefficient strongly decreases in the first stages of the wear test, reaching the lowest value among the analyzed materials (0.095). The friction coefficient remains relatively constant up to 250 m; then, it grows rapidly up to values oscillating between 0.14 and 0.16. Ultimately, CW-24 (burgundy curve) is characterized by a noticeably rocking evolution, as the friction coefficient continuously varies within the 0.14–0.19 interval without stabilizing in the investigated distance interval.

The composites' wear mechanisms were investigated through OM and CLSM (Fig. 9) and SEM (Fig. 10) analyses. The OM and CLSM images of pure copper (Figs. 9-a1, -a2) demonstrate a jagged and not coherent surface due to harsh abrasion of the surface and a possible third-body wear mechanism. The corresponding SEM images, Fig. 10-a1, -a2, -a3, also reveal the presence of delamination due to the characteristic lines

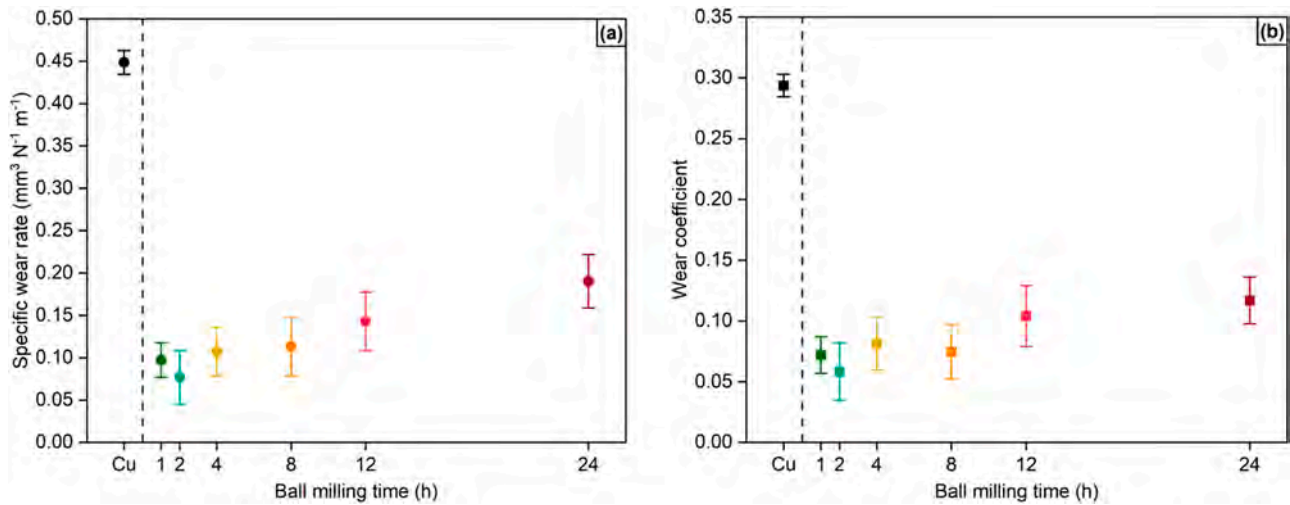


Fig. 7. (a) Specific wear rates and (b) wear coefficients from scratch tests of the CW-X composites compared with pristine Cu.

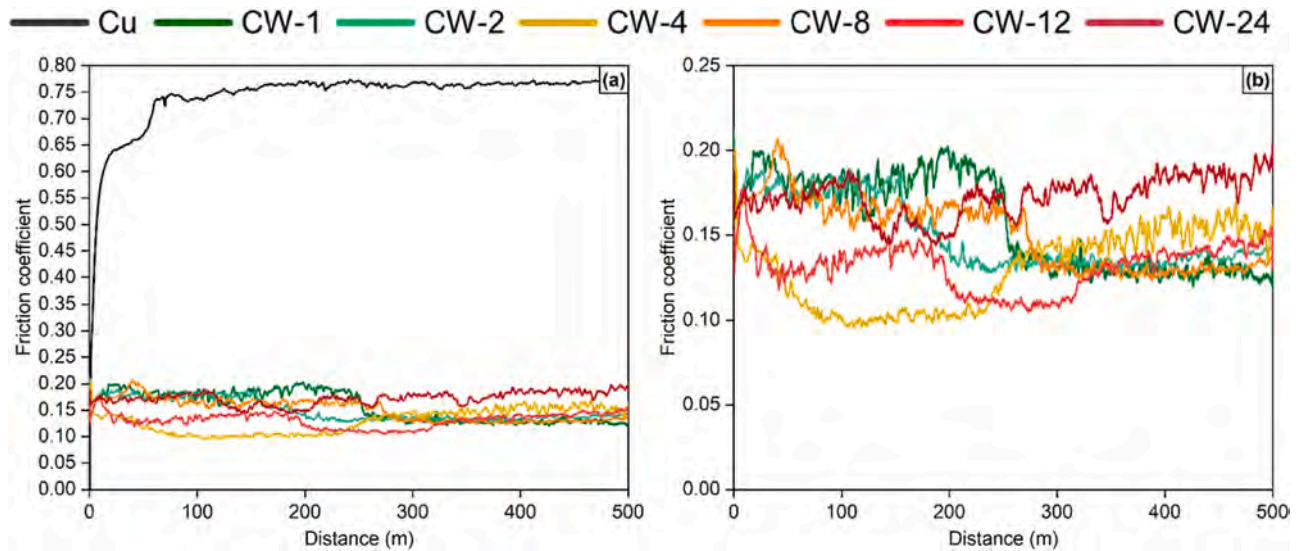


Fig. 8. (a) Friction coefficient evolution of the CW-X composites from wear tests compared with pristine Cu; (b) Close-up on the friction coefficient evolution of the CW-X composites.

perpendicular to the sliding direction and the visible detachment of thin fragments. The third-body mechanism is confirmed by the visible different wear damages that the same surface area has undergone. The wear surfaces of the composites are more homogeneous than pure copper sample. The CLSM images highlight the increase of the wear track depth at longer ball milling times (blue zones), along with the formation of smaller ridges (yellow-orange zones). In the composites' SEM images, abrasion is reduced but still visible. The detachment of particles may determine a third-body mechanism, with a consequent variation of the wear track width. By contrast, the detached particles seem relatively soft because they are flattened and overlap toward the striction portion of the track. In such a way, the piled-up particles can form a compact tribo-film within the track through which WS_2 exerts its lubricating action.

Specific wear rate and wear coefficient values from wear tests, calculated via Eqs. (8) and (9) (Section 2.6), are reported in Fig. 11. The improvement of the wear performance of the composites is visible with respect to pristine copper. Both specific wear rate and wear coefficient are quite constant up to CW-4. In particular, the lowest specific wear rate is reached by the sample CW-2 ($0.245 \pm 0.010 \times 10^{-3} \text{ mm}^3 \text{N}^{-1} \text{m}^{-1}$), while CW-4 has the lowest wear coefficient ($0.158 \pm 0.006 \times 10^{-3}$). Then,

both parameters begin to increase steeply with the ball milling time, reaching values that approach those of the pure copper sample ($0.937 \pm 0.068 \times 10^{-3} \text{ mm}^3 \text{N}^{-1} \text{m}^{-1}$ and $0.528 \pm 0.038 \times 10^{-3}$, respectively) in the case of CW-24 ($0.716 \pm 0.068 \times 10^{-3} \text{ mm}^3 \text{N}^{-1} \text{m}^{-1}$ and $0.445 \pm 0.058 \times 10^{-3}$, respectively). The detrimental effects of an excessive extension of the ball milling step on the properties of the composites may be observed, as previously inferred from electrical resistivity (Section 3.2) and scratch hardness (Section 3.3) results.

4. Discussion

Understanding the effects of ball milling time on the properties of self-lubricating Cu- WS_2 composites requires correlating the results presented in the previous sections.

The main difference in the composites originating from the analyzed ball milling times lies in the obtained microstructure, which influences the results of hardness, electrical resistivity, micro-scratch resistance, and wear behavior. The larger powder diameter highlighted for CW-24 by the granulometry analysis can be also appreciated from the OM images of its cross-section (Fig. 1), where grains are more visible with respect to the other samples. The improved degree of dispersion of the

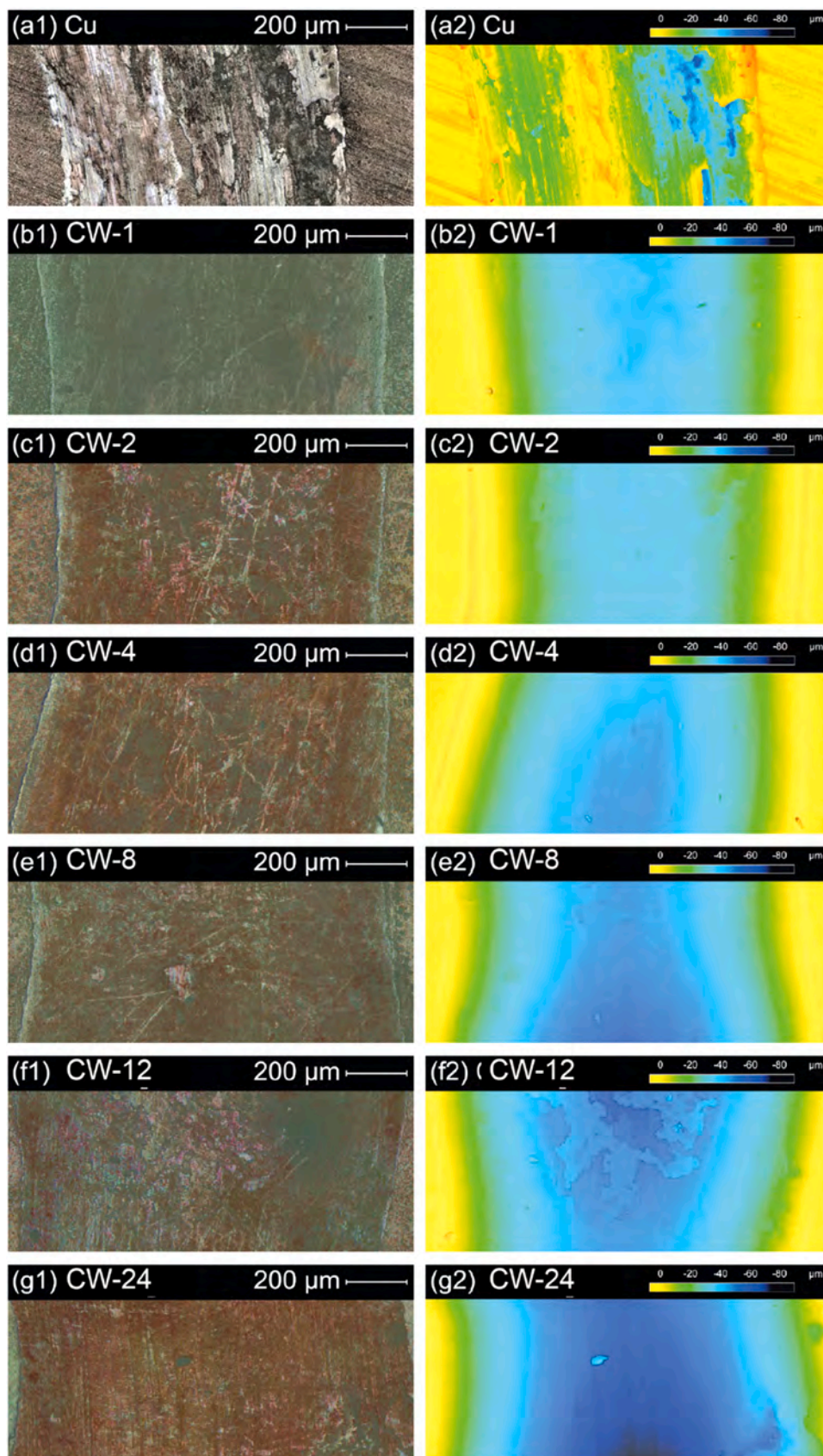


Fig. 9. Images at 20x magnification of the wear tracks: pristine Cu (a1) optical and (a2) laser; CW-1 (b1) optical and (b2) laser; CW-2 (c1) optical and (c2) laser; CW-4 (d1) optical and (d2) laser; CW-8 (e1) optical and (e2) laser; CW-12 (f1) optical and (f2) laser; CW-24 (g1) optical and (g2) laser.

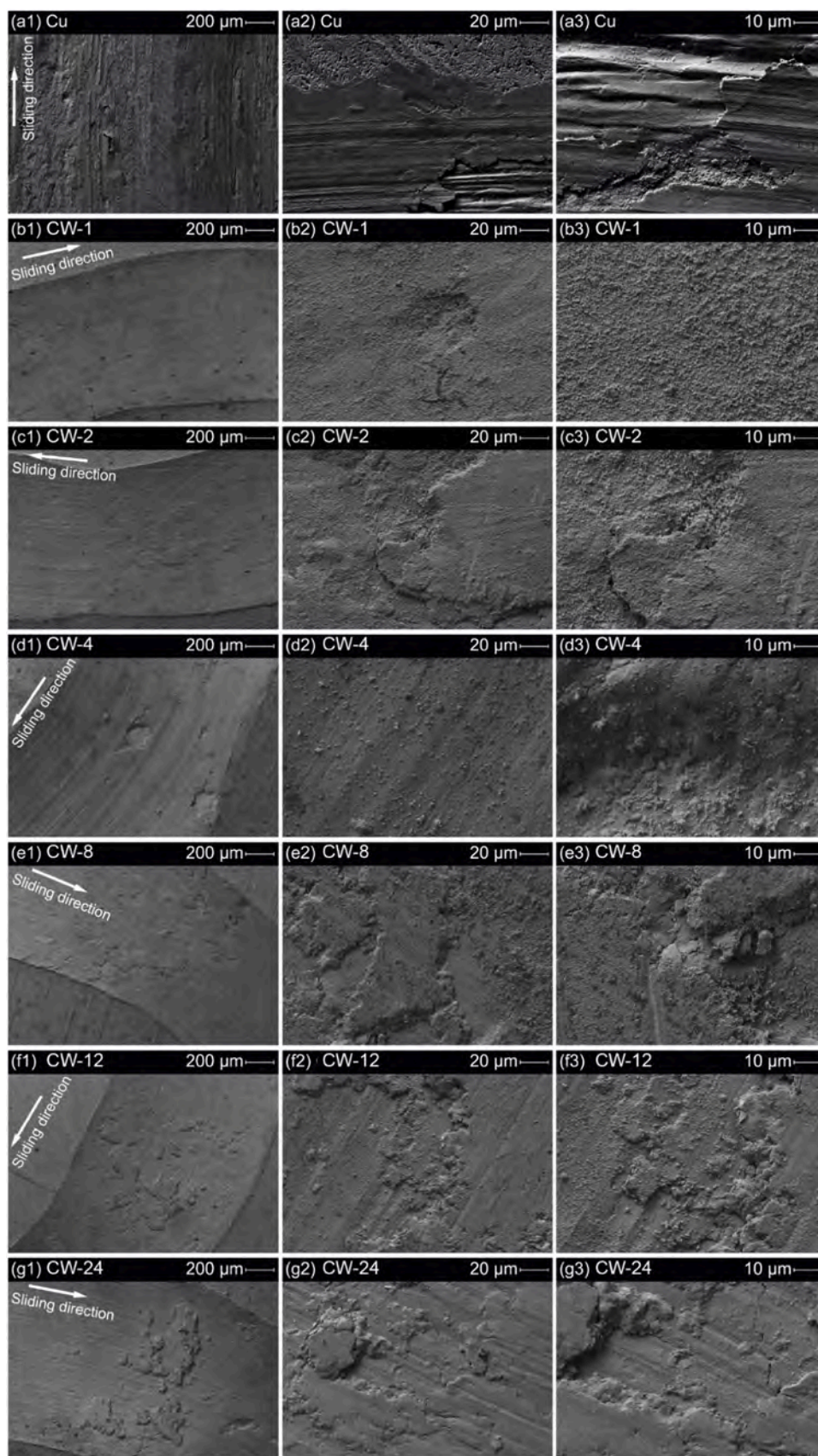


Fig. 10. SEM images of the wear tracks of pristine Cu and of the CW-X composites at different magnifications: (a) Cu, (b) CW-1, (c) CW-2, (d) CW-4, (e) CW-8, (f) CW-12, and (g) CW-24 at (1) 150x, (2) 1500x, and (3) 3000x.

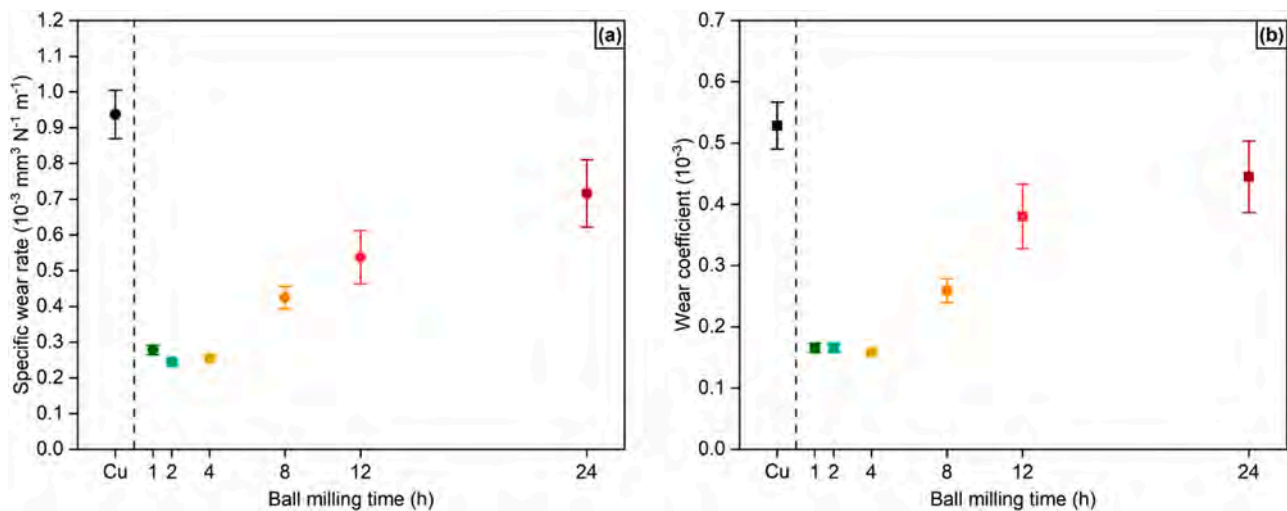


Fig. 11. (a) Specific wear rates and (b) wear coefficients from wear tests of the CW-X composites compared with pristine Cu.

solid lubricant is confirmed by the cross-sectional SEM analysis (Fig. 2). Presumably, long ball milling times promote exfoliation and blending of WS₂ layers that better disperse and stick, at first on the surface of Cu particles and then together fostering agglomeration. As a drawback, the more homogeneous distribution of small particles of semi-conductive WS₂ [82] in the copper matrix determines a shielding effect that causes a higher electrical resistivity.

The intermediate values of grinding time (i.e., 4 and 8 h) lead to the highest values of pores mean area and fraction (Fig. 3). Such an outcome could be attributed to a limited distribution of WS₂ particles, which starts to accentuate compared to CW-1 and CW-2. The decrease of agglomerates' dimension involves an increase of the interface area, which is the preferred location of porosities, as observed in the cross-sectional SEM images. Differently, pores mean area and pores fraction values of CW-12 and CW-24 diminish. A mixing time of 12 h favors the filling of empty areas by means of smaller fractions of powder, whereas a further extension up to 24 h allows the predominance of agglomeration of the composite powder with respect to the refinement of the phases and the formation of new interfaces.

The introduction of 10 wt% of solid lubricant determines a decrease in friction coefficient with respect to the pristine copper sample, both in scratch tests and wear tests. In scratch tests (Fig. 5), a slightly decreasing trend is visible with respect to the ball milling duration. Such a trend is explained by the distribution of the second phase within the copper matrix, that therefore turns out to be more readily available at the exposed surface all along with the scratch. In wear tests (Fig. 8), the friction coefficients of the composites are quite similar, especially in the second half of the test, where stabilization of the experimental system occurs. The improvement with respect to bare Cu is evident, although no specific information on the influence of the ball milling time can be derived. The main difference lies in the wear mechanisms, influenced by the microstructure determined by the different ball-milling times. A switch from a ploughing-type mechanism to a flake-like abrasive one is observed in the scratch tests, moving from short to long ball milling times based on friction coefficient and degree of penetration trends of the samples. The finer and more homogeneous distribution of the second phase may hinder optimal sintering of the copper matrix, worsening the response to scratching. Furthermore, it should be considered that a single pass of the indenter does not permit the formation of a uniform tribo-film, as it can be inferred from the wear coefficient values (between 10⁻¹ and 10⁻²), which are independent of the employed ball milling time.

A similar behavior is observed in wear tests due to the detection of abrasion scars and flake-like debris in the wear tracks. The slight transition to a combination of severe abrasion and third-body mechanism

follows the employment of longer ball milling times. The simultaneous worsening of the tribological performance is confirmed by the specific wear rate and the wear coefficient increase, albeit the presence of WS₂ mitigates the wear of the composites thanks to the formation of a compact tribo-film generated by the pile-up of detached particles.

Considering the tribological aspect, the best-expected result would be to have accessible WS₂ clusters that act as reservoirs as long as new material is exposed to the surface, spreading within the sliding contact and reducing friction and wear. Having small particles of lubricant surrounding the copper particles has two detrimental effects. First, it limits the coarsening of copper powder during sintering, and second, the amount of WS₂ available to lubricate the surface might be too little. The poor copper powder coarsening is the main reason for the observed increase in electrical resistivity, inasmuch as the electrons have a more limited path to flow through, and the scratch hardness decreases since the metallic microstructure is compromised. The latter feature makes the removal of material portions during scratching easier, aggravating the wear regimes. The friction coefficient and wear rate increase derive from the limited amount of WS₂ exposed to the surface.

5. Conclusions

This study investigated the influence of ball milling time on the fabrication of self-lubricating copper-tungsten disulfide composites via powder metallurgy. Six ball milling times (1, 2, 4, 8, 12, and 24 h) were considered, and the results were compared to pure copper.

Longer milling led to smaller second-phase micro-agglomerates and better dispersion, increasing the electrical resistivity, especially after 12 h. The friction coefficient from the scratch test slightly decreased with extended milling, shifting the wear mechanism from ploughing to flake-like. Moreover, extended milling weakened the lubricating effect of WS₂, a feature deduced from deeper wear tracks and increased wear rates due to worsened abrasive and third-body wear mechanisms.

Overall, milling beyond 12 h is detrimental to final composite properties. The optimal milling time for Cu-WS₂ composites to balance electrical conductivity, scratch resistance, and wear behavior lies between 2 and 4 h.

Declaration of Competing Interest

The authors declare the following financial interests/personal relationships which may be considered as potential competing interests: Giovanni Dotelli reports financial support was provided by EIT Raw-Materials GmbH. If there are other authors, they declare that they have no known competing financial interests or personal relationships that

could have appeared to influence the work reported in this paper.

Acknowledgments

The authors would like to thank the EIT Raw Materials, which funded this work within the project ADMA 2 – Practical training between Academia and Industry during doctoral studies (Project n. 18252), and Logic S.p.A. for supplying materials and instruments.

Appendix A. Supporting information

Supplementary data associated with this article can be found in the online version at [doi:10.1016/j.nxmate.2023.100083](https://doi.org/10.1016/j.nxmate.2023.100083).

References

- [1] R. Casati, M. Vedani, Metal matrix composites reinforced by nanoparticles—a review, *Met. (Basel)* 4 (2014) 65–83, <https://doi.org/10.3390/met4010065>.
- [2] D. Saber, K. Abd El-Aziz, A. Fathy, Corrosion behavior of copper–alumina nanocomposites in different corrosive media, *Int. J. Mech. Eng.* 5 (2016) 1–10, http://www.iaset.us/view_archives.php?year=2016&id=67&jtype=2&page=3.
- [3] Y. Afkham, R.A. Khosroshahi, R. Kheirifard, R.T. Mousavian, D. Brabazon, Microstructure and morphological study of ball-milled metal matrix nanocomposites, *Phys. Met. Metallogr.* 118 (2017) 749–758, <https://doi.org/10.1134/S00131918x17080026>.
- [4] F. Huang, H. Wang, J.-S. Chen, B. Yang, Dry ball milling and wet ball milling for fabricating copper–yttria composites, *Rare Met* 37 (2018) 859–867, <https://doi.org/10.1007/s12598-018-1086-y>.
- [5] M.K. Singh, R.K. Gautam, Dry sliding friction and wear behaviour of developed copper metal matrix hybrid composites, *Int. J. Surf. Sci. Eng.* 13 (2019) 133, <https://doi.org/10.1504/IJSURFSE.2019.102362>.
- [6] M.A. Atwater, T.L. Luckenbaugh, B.C. Hornbuckle, K.A. Darling, Solid State Foaming of Nickel, Monel, and Copper by the Reduction and Expansion of NiO and CuO Dispersions, *Adv. Eng. Mater.* 20 (2018) 1–10, <https://doi.org/10.1002/adem.201800302>.
- [7] M.A. Atwater, K.A. Darling, M.A. Tschoop, Solid-State Foaming by Oxide Reduction and Expansion: Tailoring the Foamed Metal Microstructure in the Cu–CuO System with Oxide Content and Annealing Conditions, *Adv. Eng. Mater.* 18 (2016) 83–95, <https://doi.org/10.1002/adem.201500063>.
- [8] A. Sadoun, A. Ibrahim, A.W. Abdallah, Fabrication and evaluation of tribological properties of Al₂O₃ coated Ag reinforced copper matrix nanocomposite by mechanical alloying, *J. Asian Ceram. Soc.* 8 (2020) 1228–1238, <https://doi.org/10.1080/21870764.2020.1841073>.
- [9] F. Shehata, M. Abdelhameed, A. Fathy, M. Elmahdy, Preparation and Characteristics of Cu–Al₂O₃ Nanocomposite, *Open J. Met.* 01 (2011) 25–33, <https://doi.org/10.4236/ojmetal.2011.12004>.
- [10] E. Hong, B. Kaplin, T. You, M. Suh, Y.-S. Kim, H. Choe, Tribological properties of copper alloy-based composites reinforced with tungsten carbide particles, *Wear* 270 (2011) 591–597, <https://doi.org/10.1016/j.wear.2011.01.015>.
- [11] M.I. Abd El Aal, H.S. Kim, Effect of the fabrication method on the wear properties of copper/carbon composites, *Tribol. Int.* 128 (2018) 140–154, <https://doi.org/10.1016/j.triboint.2018.07.024>.
- [12] N. Somani, Y.K. Gautam, S.K. Sharma, M. Kumar, Statistical analysis of dry sliding wear and friction behavior of Cu/SiC sintered composite, in: *AIP Conf. Proc.*, AIP Publishing LLC AIP Publishing, 2018, 020018, <https://doi.org/10.1063/1.5058255>.
- [13] S.J. Yoo, S.H. Han, W.J. Kim, A combination of ball milling and high-ratio differential speed rolling for synthesizing carbon nanotube/copper composites, *Carbon* N. Y. 61 (2013) 487–500, <https://doi.org/10.1016/j.carbon.2013.04.105>.
- [14] R. Jiang, X. Zhou, Q. Fang, Z. Liu, Copper–graphene bulk composites with homogeneous graphene dispersion and enhanced mechanical properties, *Mater. Sci. Eng. A* 654 (2016) 124–130, <https://doi.org/10.1016/j.msea.2015.12.039>.
- [15] A. Saboori, M. Pavese, C. Badini, P. Fino, A Novel Approach to Enhance the Mechanical Strength and Electrical and Thermal Conductivity of Cu–GNP Nanocomposites, *Metall. Mater. Trans. A* 49 (2018) 333–345, <https://doi.org/10.1007/s11661-017-4409-y>.
- [16] X. Zhao, J. Tang, F. Yu, N. Ye, Preparation of graphene nanoplatelets reinforcing copper matrix composites by electrochemical deposition, *J. Alloy. Compd.* 766 (2018) 266–273, <https://doi.org/10.1016/j.jallcom.2018.06.309>.
- [17] E. Chaptuill, M. Renouf, C. Zeng, Y. Berthier, Influence of Copper/Graphite Properties on the Tribological and Electrical Behavior of Copper-Graphite Third Body Layer, *Lubricants* 6 (2018) 109, <https://doi.org/10.3390/lubricants6040109>.
- [18] C. Wang, Z. Wu, F. Li, X. Gan, J. Tao, J. Yi, Y. Liu, Friction and Wear Properties of Copper Matrix Composites with CNTs/Cu Composite Foams as Reinforcing Skeletons, *Tribol. Lett.* 69 (2021) 1–7, <https://doi.org/10.1007/s11249-021-01500-3>.
- [19] J.P. Tu, Y.Z. Yang, L.Y. Wang, X.C. Ma, X.B. Zhang, Tribological properties of carbon-nanotube-reinforced copper composites, *Tribol. Lett.* 10 (2001) 225–228, <https://doi.org/10.1023/A:101666214589>.
- [20] M. Freschi, A. Arrigoni, O. Haiko, L. Andena, J. Kömi, C. Castiglioni, G. Dotelli, Physico-Mechanical Properties of Metal Matrix Self-Lubricating Composites Reinforced with Traditional and Nanometric Particles, *Lubricants* 10 (2022) 35, <https://doi.org/10.3390/lubricants10030035>.
- [21] G. Qian, Y. Feng, Y.M. Chen, F. Mo, Y.Q. Wang, W.H. Liu, Effect of WS₂ addition on electrical sliding wear behaviors of Cu-graphite-WS₂ composites, *Trans. Nonferrous Met. Soc. China (Engl. Ed.)* 25 (2015) 1986–1994, [https://doi.org/10.1016/S1003-6326\(15\)63807-9](https://doi.org/10.1016/S1003-6326(15)63807-9).
- [22] M. Moazami-Goudarzi, A. Nemati, Tribological behavior of self lubricating Cu/MoS₂ composites fabricated by powder metallurgy, *Trans. Nonferrous Met. Soc. China* 28 (2018) 946–956, [https://doi.org/10.1016/S1003-6326\(18\)64729-6](https://doi.org/10.1016/S1003-6326(18)64729-6).
- [23] Z. Yu, M. Chen, Q. Wang, X. Wang, F. Wang, Effect of Interfacial Microstructure on Mechanical and Tribological Properties of Cu/WS₂ Self-lubricating Composites Sintered by Spark Plasma Sintering, *Acta Metall. Sin. (Engl. Lett.)* 34 (2021) 913–924, <https://doi.org/10.1007/s40195-020-01187-w>.
- [24] M. Freschi, M. Di Virgilio, G. Zanardi, M. Mariani, N. Lecis, G. Dotelli, Employment of Micro- and Nano-WS₂ Structures to Enhance the Tribological Properties of Copper Matrix Composites, *Lubricants* 9 (2021) 53, <https://doi.org/10.3390/lubricants9050053>.
- [25] M. Freschi, M. Di Virgilio, O. Haiko, M. Mariani, L. Andena, N. Lecis, J. Kömi, G. Dotelli, Investigation of second phase concentration effects on tribological and electrical properties of Cu–WS₂ composites, *Tribol. Int.* 166 (2022), 107357, <https://doi.org/10.1016/j.triboint.2021.107357>.
- [26] H. Nautiyal, S. Kumari, U.S. Rao, R. Tyagi, O.P. Khatri, Tribological Performance of Cu–rGO–MoS₂ Nanocomposites Under Dry Sliding, *Tribol. Lett.* 68 (2020), 29, <https://doi.org/10.1007/s11249-020-1270-8>.
- [27] T.W. Scharf, S.V. Prasad, Solid lubricants: a review, *J. Mater. Sci.* 48 (2013) 511–531, <https://doi.org/10.1007/s10853-012-7038-2>.
- [28] H. Xiao, S. Liu, 2D nanomaterials as lubricant additive: A review, *Mater. Des.* 135 (2017) 319–332, <https://doi.org/10.1016/j.matdes.2017.09.029>.
- [29] L. Zhao, P. Yao, T. Gong, H. Zhou, M. Deng, Z. Wang, Z. Zhang, Y. Xiao, F. Luo, Effect of Adding Tungsten Disulfide to a Copper Matrix on the Formation of Tribo-Film and on the Tribological Behavior of Copper/Tungsten Disulfide Composites, *Tribol. Lett.* 67 (2019) 1–13, <https://doi.org/10.1007/s11249-019-1200-9>.
- [30] M.R. Vazirisereshk, A. Martini, D.A. Strubbe, M.Z. Baykara, Solid Lubrication with MoS₂: A Review, *Lubricants* 7 (2019) 57, <https://doi.org/10.3390/lubricants7070057>.
- [31] M. Marian, D. Berman, A. Rota, R.L. Jackson, A. Rosenkranz, Layered 2D Nanomaterials to Tailor Friction and Wear in Machine Elements—A Review, *Adv. Mater. Interfaces* 2101622 (2021), 2101622, <https://doi.org/10.1002/admi.202101622>.
- [32] G.M. Wang, S.J.C. Mpbell, A. Calka, W.A. Kaczmarek, Synthesis and structural evolution of tungsten carbide prepared by ball milling, *J. MATE RIALS Sci.* 32 (1997) 1461–1467.
- [33] Y. Wang, Y. Gao, Y. Li, C. Zhang, X. Huang, W. Zhai, Effect of milling time on microstructure and mechanical properties of Cu–Ni–graphite composites, *Mater. Res. Express* 4 (2017), 096506, <https://doi.org/10.1088/2053-1591/AA84A7>.
- [34] P. Balasubramanian, M. Battabyal, A. Chandra Bose, R. Gopalan, Effect of ball-milling on the phase formation and enhanced thermoelectric properties in zinc antimonides, *Mater. Sci. Eng. B Solid-State Mater. Adv. Technol.* 271 (2021), 115274, <https://doi.org/10.1016/j.mseb.2021.115274>.
- [35] L. Chen, H. Xie, W. Yu, Multi-walled carbon nanotube/silver nanoparticles used for thermal transportation, *J. Mater. Sci.* 47 (2012) 5590–5595, <https://doi.org/10.1007/s10853-012-6451-x>.
- [36] M.A. Morris, D.G. Morris, Ball-milling of elemental powders-compound formation and/or amorphization, *J. Mater. Sci.* 26 (1991) 4687–4696, <https://doi.org/10.1007/BF00612407>.
- [37] B.H. Lohse, A. Calka, D. Wexler, Synthesis of TiC by controlled ball milling of titanium and carbon, *J. Mater. Sci.* 42 (2007) 669–675, <https://doi.org/10.1007/s10853-006-0291-5>.
- [38] O.K. Donaldson, T.J. Rupert, Amorphous Intergranular Films Enable the Creation of Bulk Nanocrystalline Cu–Zr with Full Density, *Adv. Eng. Mater.* 21 (2019) 1–6, <https://doi.org/10.1002/adem.201900333>.
- [39] K.J. Wang, X.L. Cai, H. Wang, J. Hu, Y.F. Zhang, Preparation of Cu–Zn Alloy by Different High Energy Ball Milling, *J. Mater. Res.* 412 (2011) 259–262, <https://doi.org/10.4028/www.scientific.net/AMR.412.259>.
- [40] H. Yue, L. Yao, X. Gao, S. Zhang, E. Guo, H. Zhang, X. Lin, B. Wang, Effect of ball-milling and graphene contents on the mechanical properties and fracture mechanisms of graphene nanosheets reinforced copper matrix composites, *J. Alloy. Compd.* 691 (2017) 755–762, <https://doi.org/10.1016/j.jallcom.2016.08.303>.
- [41] M. Freschi, A. Paniz, E. Cerqueni, G. Colella, G. Dotelli, The Twelve Principles of Green Tribology: Studies, Research, and Case Studies—A Brief. Anthol., *Lubr.* 10 (2022) 129, <https://doi.org/10.3390/LUBRICANTS10060129>.
- [42] Q. Ren, G. Cui, T. Li, M. Hassani, Y. Liu, Z. Kou, High-Temperature Wear Behavior of Cobalt Matrix Composites Reinforced by LaF₃ and CeO₂, *Tribol. Lett.* 69 (2021), 149, <https://doi.org/10.1007/s11249-021-01524-9>.
- [43] J.Y. Huang, Y.K. Wu, H.Q. Ye, Ball milling of ductile metals, *Mater. Sci. Eng. A* 199 (1995) 165–172, [https://doi.org/10.1016/0921-5093\(94\)09715-1](https://doi.org/10.1016/0921-5093(94)09715-1).
- [44] A.M. Sadoun, A.F. Meselhy, A.W. Abdallah, Microstructural, mechanical and wear behavior of electrodeless assisted silver coated Al₂O₃–Cu nanocomposites, *Mater. Chem. Phys.* 266 (2021), <https://doi.org/10.1016/j.matchemphys.2021.124562>.
- [45] H. Ahmadian, A.M. Sadoun, A. Fathy, T. Zhou, Utilizing a unified conceptual dynamic model for prediction of particle size of dual-matrix nanocomposites during mechanical alloying, *Powder Technol.* 418 (2023), <https://doi.org/10.1016/j.powtec.2023.118291>.
- [46] J.Y. Huang, Y.K. Wu, H.Q. Ye, Deformation structures in ball milled copper, *Acta Mater.* 44 (1996) 1211–1221, [https://doi.org/10.1016/1359-6454\(95\)00231-6](https://doi.org/10.1016/1359-6454(95)00231-6).

- [47] M. Toozandehjani, K. Matori, F. Ostovan, S. Abdul Aziz, M. Mamat, Effect of Milling Time on the Microstructure, Physical and Mechanical Properties of Al-Al₂O₃ Nanocomposite Synthesized by Ball Milling and Powder Metallurgy, *Mater. (Basel)* 10 (2017) 1232, <https://doi.org/10.3390/ma10111232>.
- [48] D.L. Zhang, J.J. Richmond, Microstructural evolution during combustion reaction between CuO and Al induced by high energy ball milling, *J. Mater. Sci.* 34 (1999) 701–706, <https://doi.org/10.1023/A:1004504425653>.
- [49] J. Cintas, J.M. Montes, F.G. Cuevas, E.J. Herrera, Influence of milling media on the microstructure and mechanical properties of mechanically milled and sintered aluminium, *J. Mater. Sci.* 40 (2005) 3911–3915, <https://doi.org/10.1007/s10853-005-0756-y>.
- [50] C. Shuai, C. He, S. Peng, F. Qi, G. Wang, A. Min, W. Yang, W. Wang, Mechanical Alloying of Immiscible Metallic Systems: Process, Microstructure, and Mechanism, *Adv. Eng. Mater.* 23 (2021) 1–15, <https://doi.org/10.1002/adem.202001098>.
- [51] A. Fathy, M. Abdelhameed, F. Shehata, Effect of Some Manufacturing Parameters on Machining of Extruded Al-Al₂O₃ Composites, *ISRN Mater. Sci.* 2012 (2012) 1–6, <https://doi.org/10.5402/2012/748734>.
- [52] G. Romero, P. Lv, J. Huot, Effect of ball milling on the first hydrogenation of TiFe alloy doped with 4 wt% (Zr + 2Mn) additive, *J. Mater. Sci.* 53 (2018) 13751–13757, <https://doi.org/10.1007/s10853-018-2301-9>.
- [53] N.V. Ponraj, S.C. Vettivel, A. Azhagurajan, X. Sahaya shajan, P.Y. Nabhiraj, T. Theivasanthi, P. Selvakumar, A.H. Lenin, Effect of milling on dispersion of graphene nanosheet reinforcement in different morphology copper powder matrix, *Surf. Interfaces* 9 (2017) 260–265, <https://doi.org/10.1016/j.surf.2017.10.006>.
- [54] H.W. Huo, K.D. Woo, G.S. Guo, D.L. Zhang, Effect of high energy ball milling on the displacement reaction in particulate reinforced Al-Si-Cu alloy matrix composite powders, *J. Mater. Sci.* 42 (2007) 59–65, <https://doi.org/10.1007/s10853-006-1085-5>.
- [55] A. Vahid, P. Hodgson, Y. Li, Effect of High-Energy Ball Milling on Mechanical Properties of the Mg–Nb Composites Fabricated through Powder Metallurgy Process, *Adv. Eng. Mater.* 20 (2018) 1–10, <https://doi.org/10.1002/adem.201700759>.
- [56] M. Freschi, L. Dragoni, M. Mariani, O. Haiko, J. Kömi, N. Lecis, G. Dotelli, Tuning the Parameters of Cu–WS₂ Composite Production via Powder Metallurgy: Evaluation of the Effects on Tribological Properties, *Lubricants* 11 (2023) 66, <https://doi.org/10.3390/lubricants11020066>.
- [57] P. Balasubramanian, M. Battabai, A. Chandra Bose, R. Gopalan, Effect of ball-milling on the phase formation and enhanced thermoelectric properties in zinc antimonides, *Mater. Sci. Eng. B* 271 (2021), 115274, <https://doi.org/10.1016/j.mseb.2021.115274>.
- [58] Y. Wang, Y. Gao, Y. Li, C. Zhang, X. Huang, W. Zhai, Effect of milling time on microstructure and mechanical properties of Cu–Ni–graphite composites, *Mater. Res. Express* 4 (2017), 096506, <https://doi.org/10.1088/2053-1591/aa84a7>.
- [59] A.M. Sadoun, I.R. Najjar, G.S. Alsorjji, M.S. Abd-Elwahed, M.A. Elaziz, A. Fathy, Utilization of Improved Machine Learning Method Based on Artificial Hummingbird Algorithm to Predict the Tribological Behavior of Cu-Al₂O₃ Nanocomposites Synthesized by In Situ Method, *Mathematics* 10 (2022), <https://doi.org/10.3390/math10081266>.
- [60] A. Rosenkranz, M. Marian, F.J. Profito, N. Aragon, R. Shah, The use of artificial intelligence in tribology—a perspective, *Lubricants* 9 (1) (2021) 11, <https://doi.org/10.3390/lubricants9010002>.
- [61] M. Marian, S. Tremmel, Current trends and applications of machine learning in tribology—a review, *Lubricants* 9 (2021), <https://doi.org/10.3390/LUBRICANTS9090086>.
- [62] I.R. Najjar, A.M. Sadoun, A. Fathy, A.W. Abdallah, M.A. Elaziz, M. Elmahdy, Prediction of Tribological Properties of Alumina-Coated, Silver-Reinforced Copper Nanocomposites Using Long Short-Term Model Combined with Golden Jackal Optimization, *Lubricants* 10 (2022) 277, <https://doi.org/10.3390/lubricants10110277>.
- [63] A.M. Sadoun, I.M.R. Najjar, A. Fathy, M. Abd Elaziz, M.A.A. Al-qaness, A. W. Abdallah, M. Elmahdy, An enhanced Dendritic Neural Algorithm to predict the wear behavior of alumina coated silver reinforced copper nanocomposites, *Alex. Eng. J.* 65 (2023) 809–823, <https://doi.org/10.1016/j.aej.2022.09.036>.
- [64] Y.P. Jin, M. Hu, Effect of Ball Milling on Mechanical Properties of Graphite/Copper Matrix Composites, *Adv. Mater. Res.* 217–218 (2011) 936–940, <https://doi.org/10.4028/www.scientific.net/AMR.217-218.936>.
- [65] J. Grzegorek, W. Maj, Maziarz, Effect of milling time on morphology and size of copper/CNT composite powder, in: *Polish Society of Composite Materials (Ed.), Compos. Theory Pract.*, 2018, pp. 227–233.
- [66] K. Holmberg, A. Erdemir, Influence of tribology on global energy consumption, costs and emissions, *Friction* 5 (2017) 263–284, <https://doi.org/10.1007/s40544-017-0183-5>.
- [67] F.P. Bowden, D. Tabor, The Friction and Lubrication of Solids Part II, *Phys. Today* 17 (1964) 72, <https://doi.org/10.1063/1.3051671>.
- [68] P. Kurkcu, L. Andena, A. Pavan, An experimental investigation of the scratch behaviour of polymers: 1. Influence of rate-dependent bulk mechanical properties, *Wear* 290–291 (2012) 86–93, <https://doi.org/10.1016/j.wear.2012.05.005>.
- [69] P. Kurkcu, L. Andena, A. Pavan, An experimental investigation of the scratch behaviour of polymers: 2. Influence of hard or soft fillers, *Wear* 317 (2014) 277–290, <https://doi.org/10.1016/j.wear.2014.03.011>.
- [70] M. Elmahdy, G. Abouelmagd, A.A. Mazen, Investigation on microstructure and thermal properties of in-situ synthesized Cu–ZrO₂ nanocomposites, *Int. J. Mater. Res.* 108 (2017) 1103–1107, <https://doi.org/10.3139/146.111576>.
- [71] Q. Wang, M. Chen, Z. Shan, C. Sui, L. Zhang, S. Zhu, F. Wang, Comparative study of mechanical and wear behavior of Cu/WS₂ composites fabricated by spark plasma sintering and hot pressing, *J. Mater. Sci. Technol.* 33 (2017) 1416–1423, <https://doi.org/10.1016/j.jmst.2017.06.014>.
- [72] W.S. Barakat, M.I.A. Habba, A. Ibrahim, A. Fathy, O.A. Elkady, The effect of Cu coated Al₂O₃ particle content and densification methods on the microstructure and mechanical properties of Al matrix composites, *J. Mater. Res. Technol.* 24 (2023) 6908–6922, <https://doi.org/10.1016/j.jmrt.2023.05.010>.
- [73] M. Ali, A.M. Sadoun, M. Elmahdy, G. Abouelmagd, A.A. Mazen, Development and performance analysis of novel in situ Cu–Ni/Al₂O₃ nanocomposites, *Ceram. Int.* 48 (2022) 22672–22680, <https://doi.org/10.1016/j.ceramint.2022.01.287>.
- [74] M. Ali, A.M. Sadoun, G. Abouelmagd, A.A. Mazen, M. Elmahdy, Microstructure and mechanical characterization of Cu–Ni/Al₂O₃ nanocomposites fabricated using a novel in situ reactive synthesis, *Ceram. Int.* 48 (2022) 6414–6422, <https://doi.org/10.1016/j.ceramint.2021.11.185>.
- [75] D.R. Lide, S.R. Data, E.A. Board, G. Baysinger, S. Chemistry, L.I. Berger, R. N. Goldberg, B. Division, H.V. Kehiaian, K. Kuchitsu, G. Rosenblatt, D.L. Roth, D. Zwillinger, Section 12 - Properties of Solids. CRC Handb. Chem. Phys, CRC Press, 2020, pp. 2085–2322, <https://doi.org/10.1201/b17118-17>.
- [76] J.K. Xiao, W. Zhang, C. Zhang, Microstructure evolution and tribological performance of Cu–WS₂ self-lubricating composites, *Wear* 412–413 (2018) 109–119, <https://doi.org/10.1016/j.wear.2018.07.024>.
- [77] U. Erb, G. Palumbo, J.L. McCreary, The processing of bulk nanocrystalline metals and alloys by electrodeposition. Nanostructured Met. Alloy, Elsevier, 2011, pp. 118–151, <https://doi.org/10.1533/9780857091123.1.118>.
- [78] A.V. Nokhrin, N.V. Malekhonova, V.N. Chuvil' deev, N.V. Melekhin, A.M. Bragov, A.R. Filippov, M.S. Boldin, E.A. Lantsev, N.V. Sakharov, Effect of High-Energy Ball Milling Time on the Density and Mechanical Properties of W–7%Ni–3%Fe Alloy, *Met. (Basel)* 13 (2023) 1432, <https://doi.org/10.3390/met13081432>.
- [79] S.H. Whang, Introduction. Nanostructured Met. Alloy, Elsevier, 2011, pp. xxi–xxxv, <https://doi.org/10.1016/B978-1-84569-670-2.50028-9>.
- [80] C.A. Schuh, T.G. Nieh, Hardness and Abrasion Resistance of Nanocrystalline Nickel Alloys Near the Hall-Petch Breakdown Regime, *MRS Proc.* 740 (2002), 11.8, <https://doi.org/10.1557/PROC-740-11.8>.
- [81] K. Hokkirigawa, K. Kato, An experimental and theoretical investigation of ploughing, cutting and wedge formation during abrasive wear, *Tribol. Int.* 21 (1988) 51–57, [https://doi.org/10.1016/0301-679X\(88\)90128-4](https://doi.org/10.1016/0301-679X(88)90128-4).
- [82] J.A. Desai, N. Adhikari, A.B. Kaul, Chemical exfoliation efficacy of semiconducting WS₂ and its use in an additively manufactured heterostructure graphene–WS₂ –graphene photodiode, *RSC Adv.* 9 (2019) 25805–25816, <https://doi.org/10.1039/C9RA03644J>.